

UNCLASSIFIED

AD NUMBER

AD909521

LIMITATION CHANGES

TO:

Approved for public release; distribution is unlimited.

FROM:

Distribution authorized to U.S. Gov't. agencies only; Test and Evaluation; 23 FEB 1973. Other requests shall be referred to Naval Weapons Center, China Lake, CA.

AUTHORITY

usnwc ltr, 30 aug 1974

THIS PAGE IS UNCLASSIFIED

AD909521 L

NWC TP 5493

# Inelastic Low-Energy Electron Diffraction Measurements on Al(111)

by  
J. O. Porteus  
and  
W. N. Faith  
*Research Department*



## Naval Weapons Center

CHINA LAKE, CALIFORNIA ■ MARCH 1973



Distribution limited to U.S. Government agencies only; test and evaluation; 23 February 1973. Other requests for this document must be referred to the Naval Weapons Center.

NWC Technical Publication 5493

Published by . . . . . Research Department  
Collation . . . . . Cover, 7 leaves, DD Form 1473, abstract cards  
First printing. . . . . 50 unnumbered copies  
Security classification . . . . . UNCLASSIFIED

# Naval Weapons Center

AN ACTIVITY OF THE NAVAL MATERIAL COMMAND

H. Suerstedt, Jr., RADM, USN ..... Commander  
H. G. Wilson ..... Technical Director

---

## FOREWORD

In order to carry out its responsibilities and missions the Navy has a vital, continuing interest in the science and technology of weapons systems components. Successful development of laser optical, and solid-state electronic devices, for example, depends on specialized knowledge of the relevant physical characteristics of surfaces and thin films. One very important characteristic is the nature of the electronic excitations which result from the presence of the surface, and which are strongly influenced by surface conditions. Such excitations not only play a direct role in the optical, and electronic transport properties, but also show promise as a gauge of surface quality. The surface plasmon is an excitation of this kind. Its dispersion (energy vs. momentum) and lifetime are known to be sensitive to surface roughness and to thin contaminating layers. Although surface plasmons may be investigated by optical methods, such methods lack the spatial resolution needed to explore the very small scale roughness and crystallographic effects which are believed to be of great importance in optical scattering. An alternative method which provides the necessary resolution is inelastic low energy electron diffraction (ILEED). Recent advances in the development of ILEED as a new surface research tool are reported in the following reprint published in the Journal of Vacuum Science and Technology, Vol. 9, May-June 1972.

This work was supported by the Naval Material Command, Director of Laboratory Programs, under Project No. ZR 00001, Task Area No. ZR 01102. Continuing work in this area is supported in part by the Advanced Research Projects Agency under Order No. 2175.

Released by  
HUGH W. HUNTER, Head  
Research Department  
23 February 1973

Under Authority of  
H. G. WILSON  
Technical Director

# Inelastic Low-Energy Electron Diffraction Measurements on Al (111)

J. O. Porteus and W. N. Faith

*Michelson Laboratory, Physics Division, China Lake, California 93555*

(Received 8 September 1971; in final form 17 January 1972)

An experimental study has been made of electrons in the energy range 40–80 eV, inelastically scattered and diffracted from a clean Al(111) surface. The surface is prepared by epitaxial vapor deposition on a Si(111) single-crystal surface in ultrahigh vacuum immediately preceding the measurements. The inelastic electron intensity at a given energy loss and angle is obtained as the energy derivative of the amplified electron current from a Faraday collector having a retarding field analyzer and limited angular acceptance. The energy derivative comes from the digitally computed average of a repeatedly measured difference in dc signal accompanying a fixed increment in retarding field. Using this method inelastic angular and loss profiles at 15° incidence have been obtained in the vicinity of a Bragg maximum of the 00 elastic beam. The profiles show structure related to the surface and volume plasmon momenta by a two-step model of inelastic diffraction. Dispersion data inferred by applying this model to the "loss-before-diffraction" structure are compared with results from other sources. The surface plasmon dispersion obtained from inelastic low energy electron diffraction measurements shows promise as a new means of characterizing solid crystalline surfaces.

## Introduction

Inelastic low energy electron diffraction (ILEED) offers a promising new means of relating the properties of surface-sensitive electronic excitations to surface crystallography. Unlike optical photons, electrons in the energy range 10–100 eV produce collective excitations for which the wave vector  $K$  is commonly in the range 0.1–1 Å<sup>-1</sup>. Such excitations, especially the surface plasmons, which penetrate as  $e^{-Kz}$ , can characterize a seldge only a few atomic layers deep. Also, the information is obtained selectively from those areas of the sample which are sufficiently well ordered to produce a LEED pattern, and therefore have a well-defined lattice structure at the surface. In the latter respect ILEED differs basically from both optical and kilovolt electron transmission experiments.

It is only within the past two years that the role of excitation momentum in ILEED has been fully recognized. Because of instrumental limitations, especially the large collector acceptance angles used in earlier studies, ILEED maxima were found to coincide with the elastic Bragg maxima when allowance was made for the energy loss. However, studies on a tungsten (110) surface, using high angular resolution, showed small deviations from coincidence which could be attributed to the excitation momenta.<sup>1,2</sup> Similar results have since been observed using a silver (111) surface.<sup>3</sup> These experimental results, along with recent developments in LEED, stimulated the development of a theory of ILEED intensities, including momentum considerations.<sup>4,5</sup> Predictions were given for Al(100), where the plasmon modes are comparatively well known and the diffraction is relatively kinematic. Qualitative experimental confirmation of this theory has been reported, using an epitaxially prepared Al(111) surface.<sup>6</sup> This

paper describes these measurements in detail in terms of a kinematic two-step model.<sup>2,5</sup> Some implications of the measurements in terms of recent intensity calculations on Al(111) are described elsewhere.<sup>7,8</sup>

## I. Model

Attention is restricted here to the azimuth containing the 00 LEED beam. Our principal interest is in the variation of inelastically diffracted intensity within this azimuth as the polar angle is scanned. When all other diffraction variables remain fixed, the result of this scan is called an angular profile or, more specifically, a polar angular profile. Other types of diffraction profiles, which are of secondary interest here, are generally labeled by the scanned variable, all other variables remaining fixed. Profiles in which the energy loss remains fixed are classified either as elastic or inelastic, depending, respectively, on whether the energy loss is nominally equal to zero or not.

For each type of plasmon two cases of the two-step model must be considered, i.e., diffraction followed by loss (DL) and loss followed by diffraction (LD). Each of these cases can act in conjunction with Bragg diffraction to give rise to two ILEED maxima in an angular profile. These correspond to the two possible directions (in the given azimuth) of the component of plasmon momentum parallel to the surface. For each Bragg peak a given excitation should therefore produce a total of four distinct ILEED maxima in the sequence of angular profiles at different primary energies. These maxima are quite well defined for the surface plasmon (Fig. 5 of Ref. 4) and somewhat less so for the bulk plasmon (Fig. 4 of Ref. 4). Since the momentum associated with the surface plasmon is constrained to the surface plane, the positions of the ILEED maxima are well determined in

the angular profiles by the fixed energy loss, conservation of energy, conservation of momentum parallel to the surface, and the dispersion relationship between plasmon momentum and energy. Conservation of the momentum component normal to the surface is relatively unimportant as a result of the small mean-free path for inelastic collisions ( $\lesssim 10$  Å in Al). The bulk plasmon case is complicated by the fact that the plasmon momentum is not constrained to the surface plane. The resulting lack of fixed momentum exchange for given energy loss eliminates the condition leading to the well-defined beams in the surface plasmon case. However, the vestige of normal momentum conservation, combined with strict conservation of parallel momentum, provides a relaxed condition for intensity maxima which produces some structural definition. The resulting momentum-tuned side bands<sup>4,5</sup> are the basis of our earlier excitation dispersion determinations for tungsten.<sup>2</sup> An additional consideration for the bulk plasmon, which is not included in the basic two-step model, is the possibility of coherence between the DL and LD processes. This may introduce additional conditions for inelastic diffraction in the form of sidebands in the inelastic primary energy profile.<sup>6</sup> Typically, two peaks representing DL and LD split into four. Since this energy profile is simply a cross section of the angular profiles at constant exit angle, such splitting should be apparent in the angular profile data. This effect does not appear in the present data and will not be considered here.

### A. Surface Plasmon

Analyses of the DL and LD processes for the surface plasmon are made with reference to Figs. 1(a) and 1(b), respectively, which illustrate wave-vector relationships in the reciprocal lattice plane containing the 00 LEED beam. Energy conservation requires that

$$E_p - E_s = E(K), \quad (1)$$

where the plasmon energy  $E$  is equal to the fixed energy loss in the sequence of angular profiles at different primary energies. This implies that the plasmon momentum  $\mathbf{K}$  is also fixed in magnitude, and is related to the energy loss through the dispersion relationship  $E(K)$ . The primary and secondary electron energies of the interacting electron are related to the corresponding free-electron wave vectors  $\mathbf{k}_p$  and  $\mathbf{k}_s$  (kinematic approximation), by

$$E_p = (\hbar^2/2m)k_p^2, \quad (2)$$

$$E_s = (\hbar^2/2m)k_s^2. \quad (3)$$

The magnitude of  $\mathbf{k}_s$  is therefore governed by the primary energy and fixed loss as indicated by the arcs in Fig. 1. Momentum conservation requires that

$$\mathbf{G} = \mathbf{k}_d - \mathbf{k}_i, \quad (4)$$

and

$$k_d = k_i, \quad (5)$$

where  $\mathbf{G}$  is the reciprocal lattice vector  $\mathbf{OP}$  (including  $2\pi$ )

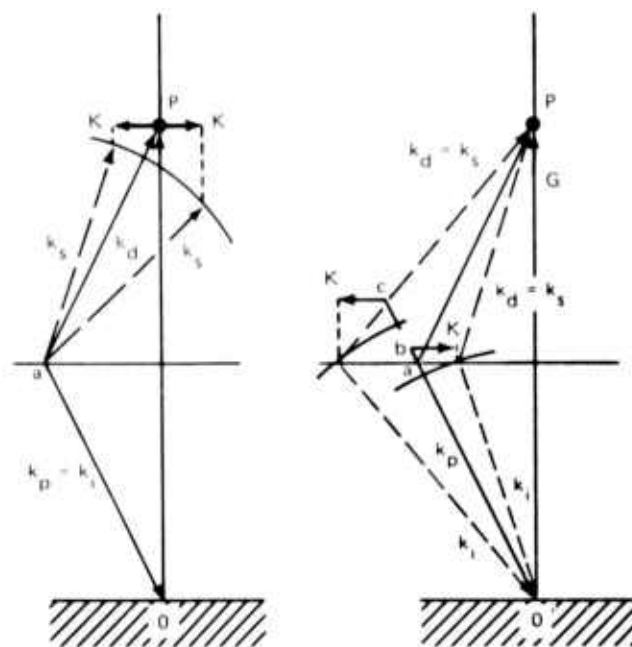


FIGURE 1. Wave vector relationships in the two-step model for surface plasmon LEED maxima in the inelastic angular profiles near an elastic 00 Bragg maximum. The 00 reciprocal lattice rod is normal to the sample surface, as indicated. Long solid vectors  $\mathbf{aO}$  and  $\mathbf{aP}$  represent the incident and diffracted LEED beams, respectively. Short horizontal vectors represent the surface plasmon. Diffraction before loss (DL) is represented in (a). Here an ILEED doublet (dashed vectors  $\mathbf{k}_i$ ) occurs when the primary electron wave vector  $\mathbf{k}_p$  corresponds to  $\mathbf{aO}$ . Loss before diffraction (LD) is represented in (b). Here two inelastic maxima (dashed vectors  $\mathbf{k}_d = \mathbf{k}_i$ ) are produced at higher primary energies, when  $\mathbf{k}_p$  corresponds to  $\mathbf{bO}$  or to  $\mathbf{cO}$ .

corresponding to the Bragg energy observed in the elastic primary energy profile;  $\mathbf{k}_i$  and  $\mathbf{k}_d$  represent the incident and diffracted electron wave vectors defining the diffraction step of the two-step process. Neglecting refraction arising from the inner potential,<sup>2</sup> DL and LD correspond to

$$\mathbf{k}_i = \mathbf{k}_p \quad (\text{DL}) \quad (6a)$$

and

$$\mathbf{k}_d = \mathbf{k}_s \quad (\text{LD}), \quad (6b)$$

respectively. Conservation of parallel momentum in the scattering step requires

$$k_i \sin\theta_i - k_d \sin\theta_d = K \sin\theta \quad (\text{DL}) \quad (7a)$$

and

$$k_i \sin\theta_i - k_p \sin\theta_p = K \sin\theta \quad (\text{LD}), \quad (7b)$$

respectively, where the  $\theta$ 's represent the direction angles of wave vectors with corresponding subscripts;  $\theta$  alone applies to the plasmon wave vector  $\mathbf{K}$ . All angles are referred to the normal. Since the surface plasmon wave vector is constrained to the surface plane,

$$\sin\theta = \pm 1. \quad (8)$$

The above equations will be used to predict the LEED data in two different ways. In the first approach we adopt the dispersion relationship

$$E(K) = 10 + 4K + 3K^2, \quad (9)$$

where  $E$  is in electron volts, and  $K$  in  $\text{angstrom}^{-1}$  units.

TABLE I. Surface plasmon ILEED maxima. Al(111), 00 beam,  $\phi=0^\circ$ ,  $\theta_p=15^\circ$ .

Process	$E(K)$	$K(\text{\AA}^{-1})$	Eq. (9)		$K(\text{\AA}^{-1})$	Eq. (10)		Observed	
			$E_p(\text{eV})$	$\theta_s(\text{deg})$		$E_p(\text{eV})$	$\theta_s(\text{deg})$	$E_p(\text{eV})$	$\theta_s(\text{deg})$
DL	8.4				0.32	51	11	50	11
LD						51	22	50	(18)
						58	11	60	11
						63	21		
DL	10.4	0.09	51	15.2	0.25	51	12.4	50	13
			51	18.6		51	21.4	50	19
LD			61	15.0		60	12.5	60	12.5
			63	18.0		65	20.4		
DL	12.4	0.45	51	9	0.48	51	8	55	8
			51	26		51	27	(55)	16
LD			61	9		61	9	(60-65)	9
			69	24		70	24		
DL	14.4	0.72	51	4	0.71	51	4	(50-55)	(5)
			51	32		51	32		
LD			62	5.4		62	5.5	60	5.5
			75	28		75	28		
DL	16.4	0.94	51	0	0.82	51	3	(50-55)	6
			51	39		51	36	50-55	15
			64	2		64	4	60	4
LD			81	31		79	29		

The first term is derived from high-energy electron loss experiments on clean Al,<sup>9</sup> and the coefficients in the second and third terms are from theory<sup>10</sup> since no experimental values other than those derived from the present data are yet available. Using the appropriate members (a) or (b) of Eqs. (6) and (7), the above equations are solved simultaneously to predict  $E_p$  and  $\theta_s$ , which are tabulated under Eq. (9) in Table I for  $E > 10$  eV.

In the second approach we use Eqs. (1)–(5), (6b), and (7b) to derive an expression for  $K$  in terms of the observed LD peak positions,

$$K = (\hbar^2/2m)^{-1/2} |(E_s)^{1/2} \sin\theta_s - (E_p)^{1/2} \sin\theta_p|. \quad (10)$$

This is the surface plasmon form of Eq. (13), Ref. 2, for diffraction by the 00 reciprocal lattice rod. As in the

past,<sup>2</sup> we choose the prominent LD peak for the derivation of  $K$  since its position can usually be measured with greater precision than that of the DL maxima. As present results will show, the latter maxima are comparatively weak; moreover, they occur at the Bragg energy, where the noise level from the superimposed elastic intensity is relatively high. Since the  $E_p$  interval between our observed angular profiles is somewhat large (5 eV) for an accurate determination of the LD peak energy value to be used in Eq. (10), we introduce

$$E_s = E_{00l}(\theta_p) (\cos^2\theta_p / \cos^2\theta_s), \quad (11)$$

which follows from the model [cf. Fig. 1(b)]. Here  $E_{00l}(\theta_p)$  is the Bragg energy from the elastic primary energy profile measured at primary angle  $\theta_p$ . Four conditions must be simultaneously satisfied: Eqs. (1), (10),

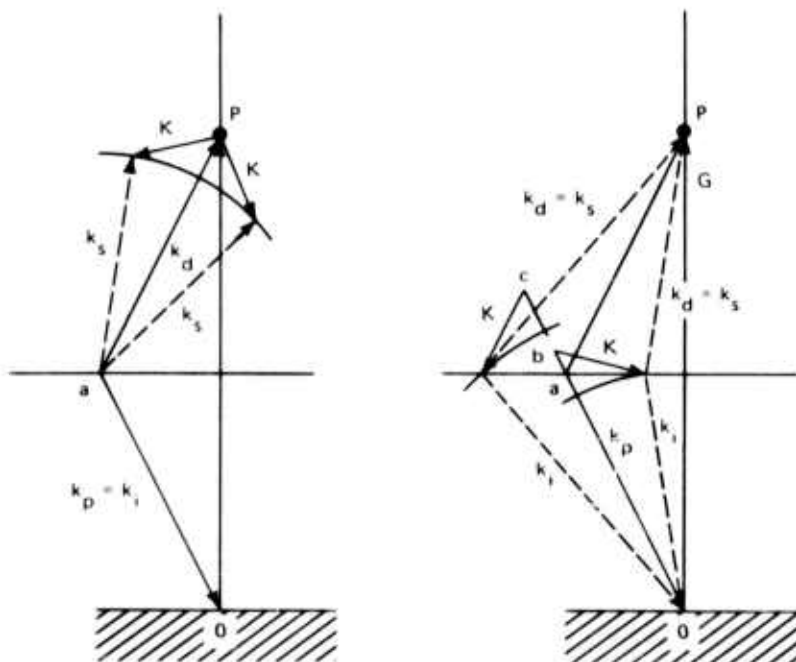


FIGURE 2. Wave vector relationships in the two-step model for bulk plasmon ILEED maxima in the inelastic angular profiles near an elastic 00 Bragg maximum. Terminology and representation of DL and LD processes are analogous to Fig. 1. Notice that  $K$  is no longer constrained to the surface plane and that the vestige of the normal momentum component is now conserved.

TABLE II. Bulk plasmon ILEED maxima. Al(111), 00 beam,  $\phi = 0^\circ$ ,  $\theta_p = 15^\circ$ .

Process	$E(K)$	$K(\text{\AA}^{-1})$	Eq. (13)		Eqs. (14), (15)			Observed	
			$E_p(\text{eV})$	$\theta_s(\text{deg})$	$K(\text{\AA}^{-1})$	$E_p(\text{eV})$	$\theta_s(\text{deg})$	$E_p(\text{eV})$	$\theta_s(\text{deg})$
DL	14.4				0.49			(50)	14.5
LD						65	14	65	14
DL	16.4	0.68	51	11.5	0.60			65	11.5
			51	19					
LD			65	9		70	19		
			71	21					
DL	18.4	1.06	51	28	0.74			70	9
			51	17					
			67	9					
LD			75	27		73	21		

(11), and the  $\theta_s$  vs  $E_p$  dependence of the LD peak, which is inferred from the angular profiles at the given energy loss  $E$ . Having obtained  $K$  in this manner, we proceed as with Eq. (9) to predict the positions of the weaker maxima. Results are tabulated in Table I under the heading Eq. (10).

## B. Bulk Plasmon

Figures 2(a) and 2(b) show wave vector relationships for the bulk plasmon corresponding to those shown in Fig. 1. Equation (8) does not apply here; instead, the ILEED maxima are determined by the vestige of momentum conservation normal to the surface, which may be expressed as

$$k_d \cos\theta_d - k_s \cos\theta_s = K \cos\theta \quad (\text{DL}), \quad (12a)$$

$$k_p \cos\theta_p - k_s \cos\theta_s = K \cos\theta \quad (\text{LD}) \quad (12b)$$

in the cases indicated.

We again provide two types of predictions from the model. The first is based on the bulk plasmon dispersion observed with high energy electrons,<sup>9</sup>

$$E(K) = 15 + 3.048K^2. \quad (13)$$

The second is based on a determination of  $K$  from the data, using the model of Fig. 2(b), which yields<sup>2</sup>

$$K = (\hbar^2/2m)^{-1/2} \csc\theta [(E_s)^{1/2} \sin\theta_s - (E_p)^{1/2} \sin\theta_p], \quad (14)$$

where

$$\theta = \arctan \left\{ \frac{[(E_s)^{1/2} \sin\theta_s - (E_p)^{1/2} \sin\theta_p]}{[(E_p)^{1/2} \cos\theta_p - (E_s)^{1/2} \cos\theta_s]} \right\}. \quad (15)$$

Equations (14) and (15) are applied to the prominent LD peak positions. The procedure is analogous to that described above for the surface plasmon, and results are similarly presented in Table II.

## II. Experiment

### A. Diffractometer

Our diffractometer is the scanning collector instrument used in previous work.<sup>1,2</sup> Approximate over-all angular and energy resolutions are  $2^\circ$  and 0.5 eV, respectively. The gas source has been replaced with an

aluminum evaporator, and a (111)-oriented Si single crystal slice now occupies the sample holder, thus permitting preparation of an Al(111) surface by epitaxial vapor deposition. The vapor source consists of a BN crucible, externally threaded to accommodate a helix of tungsten heater wire. A BN sleeve covers the helix for heat retention. The charge, consisting of 99.999% aluminum wire, is supported on an externally manipulated hook above the crucible until the latter has been thoroughly outgassed, as determined by residual gas analysis. This procedure permits evaporation in the low  $10^{-9}$  range at a deposition rate of 100  $\text{\AA}/\text{min}$ .

### B. Sample Preparation

The sample preparation procedure was developed by Bauer,<sup>11</sup> using a standard three-grid LEED system equipped with modulation and lock-in detection for Auger analysis. Surface cleanliness and ordering of the epitaxially grown Al(111) films were found to be at least comparable to those of single crystal samples prepared by argon ion bombardment and annealing.<sup>12</sup> The substrate is of device-grade Si, ground and polished to within  $0.05^\circ$  of the 111 axis using SiC abrasive followed by diamond paste. A chemical etch consisting of 1 part HF to 3 parts  $\text{HNO}_3$  is followed by rinses in distilled water and alcohol. Final cleaning by heating to a maximum temperature of  $1200^\circ\text{C}$  produced the Si-7 $\times$ 7 pattern. After establishing a constant evaporation rate of Al the cleaned Si is exposed without heating for 6 min, followed by a 10-min anneal at  $\sim 400^\circ\text{C}$ . The resulting Al films have an average thickness of  $\sim 600 \text{\AA}$ ; the LEED pattern is Al(111) 1 $\times$ 1 with no evidence of the Si pattern. All measurements are made at  $2 \times 10^{-10}$  Torr, or better, within 3 h of sample preparation. Before each data run the sample was renewed by flashing off the old aluminum and redepositing. Except for an increase in peak-to-background intensity with each successive deposition, the LEED pattern and inelastic data are quite reproducible. The aging effect is attributed to an increase in diffracting area of the sample as a result of aluminum-induced surface migration of Si atoms during the heating for aluminum removal. This is supported by the micrograph of Fig. 3, which shows the portion of the sample exposed to aluminum as having a higher pro-

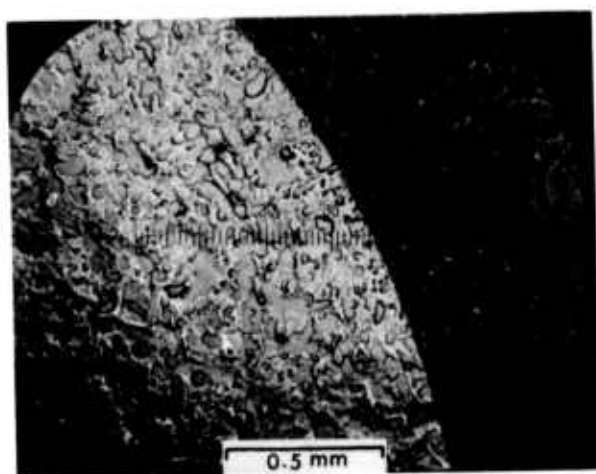


FIGURE 3. Optical micrograph of typical sample surface. The darker area is bare Si substrate, which was obscured from the Al vapor beam. Diffraction is believed to occur only from the small flat areas, which occupy a larger fraction of the surface in the Al-covered portion.

portion of apparently flat areas compared to the unexposed portion.

### C. Measurement Procedure

Since the inelastic signal is only of the order of 1% of the peak elastic signal, and data acquisition time must be minimized to avoid sample contamination, a highly sensitive and efficient data collection system is required for the inelastic measurements. Figure 4 shows a flow chart of the system used here. Amplification of the collector current is performed by a Cary model 36 vibrating-reed amplifier, which has an inherent noise

level in the  $10^{-15}$  Å range for a 0.1-sec response time. To obtain a given data point, stepwise changes in the collector's retarding field are initiated by an advance pulse from a Vidar 5203 digital data acquisition system to a voltage stepper. The latter provides programmable electronic switching of resistances in the control circuit of a dc power supply, whose output is applied directly to the collector guard electrode. Stepping is confirmed by a retaining record command pulse from the stepper, which causes digital encoding and tape recording of the amplified collector signal after a 0.3-sec settling time. The next advance pulse is produced on completion of recording. The stepping mode is equivalent to square wave modulation of the retarding potential at 1.7 Hz, 0.8 eV peak to peak. A digital computer, which analyzes the tape, computes the average signal difference between half-cycles over 15 or more cycles for the data point, and thereby performs the demodulation. In addition, the rms deviation, or noise level, is computed; printout and point-by-point data plotting with error bars are optional outputs.

Resetting the diffractometer for a new data point is largely automatic. The retard voltage stepper may be programmed for a complete loss profile scan, including advancement of the energy loss by 0.4 eV between data points. For an angular profile the collector angle is mechanically stepped two degrees on a manual command. For elastic energy profiles the output of the vibrating-reed amplifier is applied directly to the Y axis of an XY plotter. The X axis of the plotter, which corresponds to the primary beam voltage, is scanned continuously.

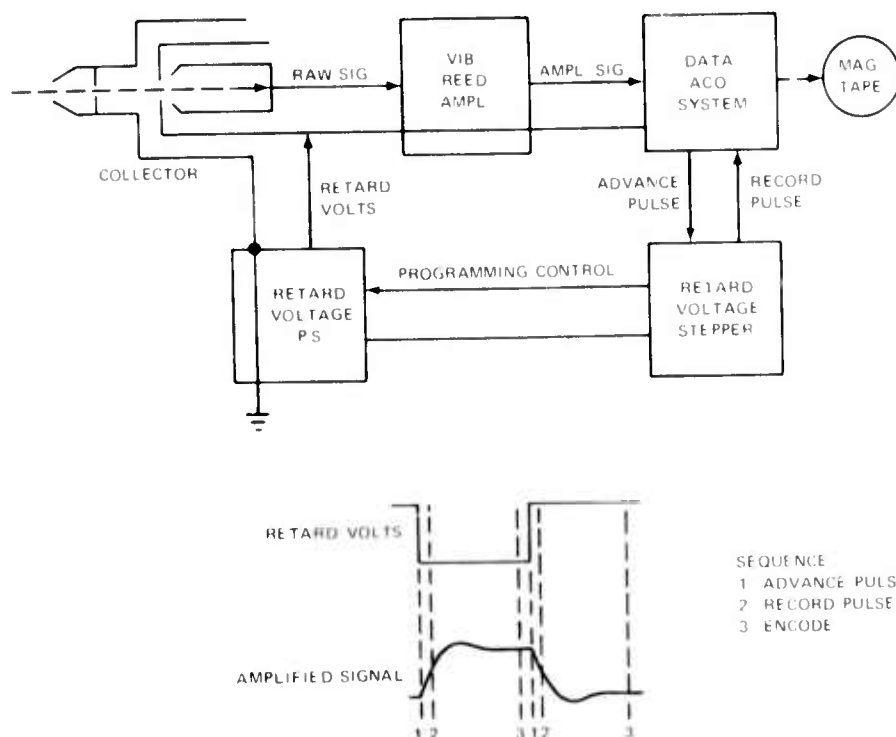


FIGURE 4. Flow chart and timing sequence of data collection system.

### III. Results and Discussion

#### A. Elastic Primary Energy Profile

An elastic primary energy profile of the 00 LEED beam from our sample at  $\theta_p = 15^\circ$  in the azimuth  $\phi = 0^\circ$  of the 10 LEED beam<sup>13</sup> is shown in Fig. 5. These settings are the same as for the other types of profiles discussed below. The structural features, which exhibit sixfold azimuthal symmetry as a result of reciprocity, generally correspond to those reported for single crystal Al(111).<sup>13</sup> However, two of the major peaks appear at the somewhat lower energies of 51 and 102 eV in our data. The position of our 28-eV peak is in better agreement, but is also less accurate, as a result of rapidly varying incident intensity at this energy. With regard to the inelastic data, attention will be focussed on structure related to the 51-eV Bragg peak, although some influence of the other two prominent peaks is also present.

#### B. Loss Profiles

Figure 6 gives the energy-loss distribution of scattered electrons, i.e., loss profile, measured in the specular direction at the approximate energy of the 51-eV Bragg maximum in the 00 LEED beam. The loss profiles, in conjunction with the angular profiles, are useful in identifying the origin of HLEED structure and in assessing the effects of broadening due to plasmon damping.<sup>5</sup> Except for excitation momentum considerations, the contribution from DL processes is a maximum here for all values of the energy loss, whereas the LD contribution becomes large only as the energy loss approaches zero. Proceeding upward from the strong elastic component at zero loss, one first finds a back-

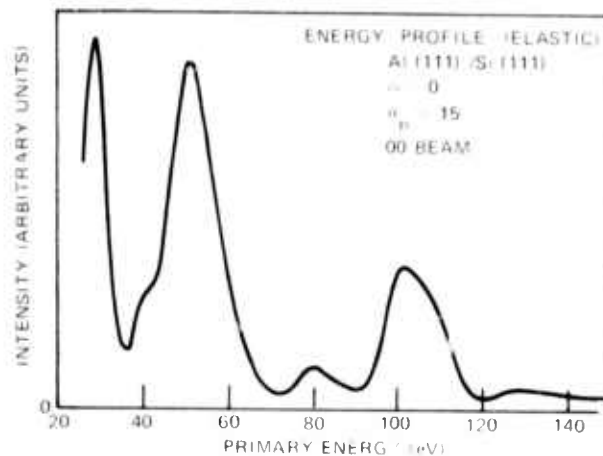


FIGURE 5. Elastic primary energy profile corresponding to present inelastic measurement situation.

ground scattering component whose intensity decreases with increasing loss. This arises mainly from one-electron excitations of low energy, possibly including interband transitions which have been observed in the optical data.<sup>14</sup> Going higher in energy loss one finds a prominent peak at 10.2-eV loss which is produced by excitation of the surface plasmon. The smaller peak at 14.6-eV loss arises from the bulk plasmon.

In the loss profiles shown in the next two figures the primary energy has been increased to 60 eV and the collector is out of the specular direction by  $5^\circ$  in polar angle, toward the normal in Fig. 7 and away from it in Fig. 8. The most striking feature on comparison of these two figures is the gross angular asymmetry of intensity of the surface plasmon peak, in spite of the symmetrical

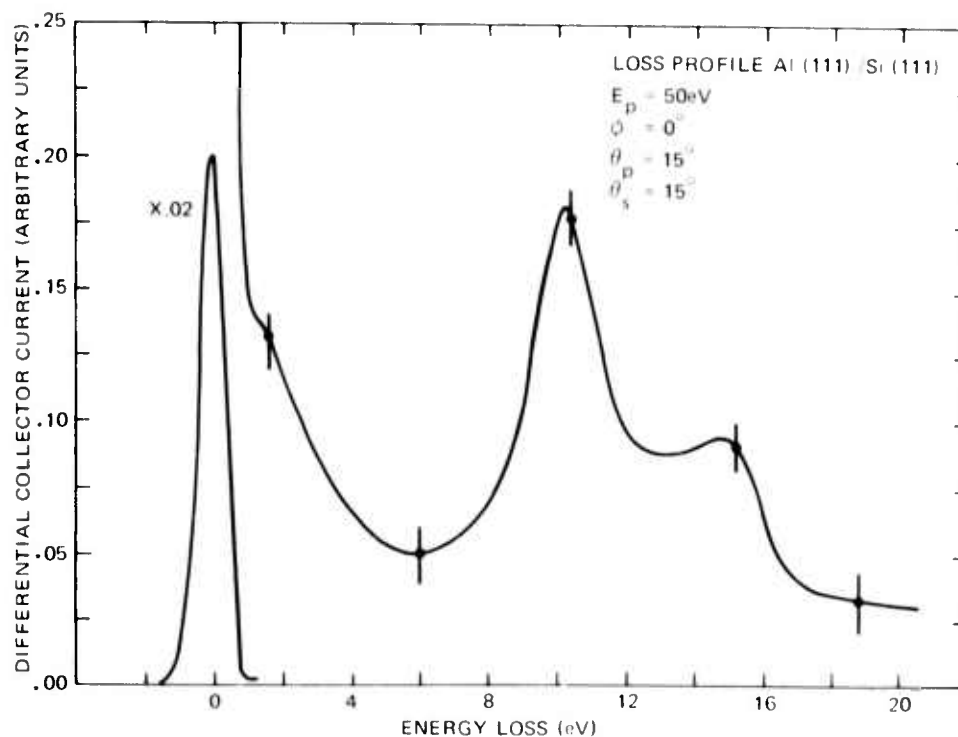


FIGURE 6. Loss profile measured in direction of the 00 beam at a Bragg maximum. Typical data points are shown with error bars representing rms deviation.

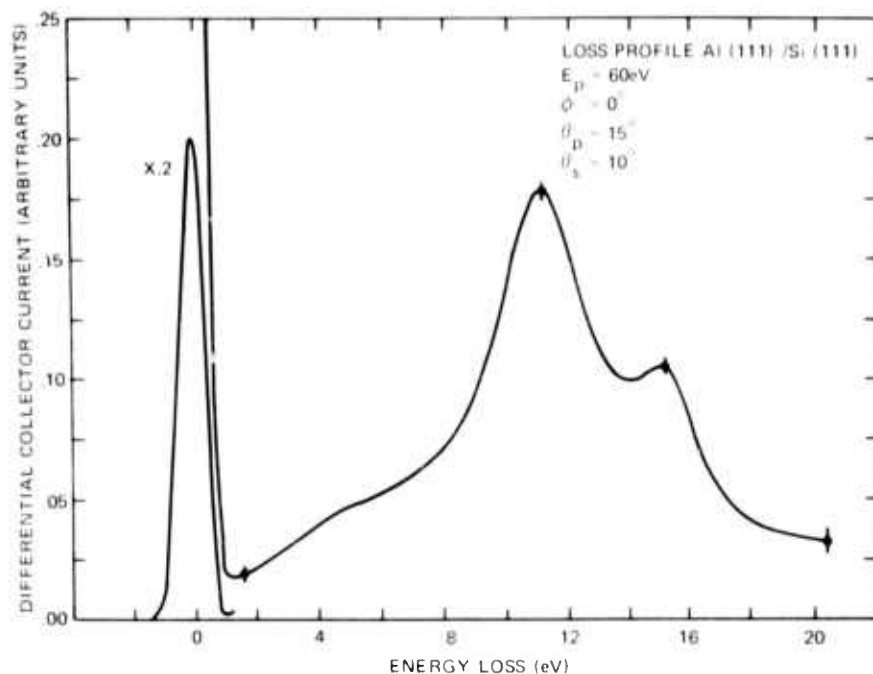


FIGURE 7. Loss profile with collector set  $5^\circ$  from the 00 beam in the direction of the normal. The primary energy is 10 eV greater than in Fig. 6.

placement of the collector relative to the LEED beam. By increasing the primary energy to 9 eV above the 51-eV Bragg maximum, the DL and low loss LD contributions have been suppressed in favor of LD contributions having energy loss near 9 eV; hence, the strong involvement of the surface plasmon. The asymmetry is a manifestation of the plasmon momentum, as represented in Fig. 1(b) (primary wave vector  $b_0$  and the plasmon wave vector directed toward the right of the figure). Another interesting feature of Fig. 7 is that the surface plasmon peak lies  $\sim 1$  eV higher in energy loss than in Fig. 6. This results from the surface plasmon dispersion: As is apparent from Fig. 1, the greater the departure of an ILEED maximum from the LEED beam, the greater the plasmon momentum. The collector in Fig. 7 thus samples a higher point on the dispersion curve. The fact

that the peak shifts to higher energy loss is indicative of a positive dispersion, i.e., the surface plasmon energy increases with increased momentum. While plasmon momentum effects and dispersion are evident in the loss profiles, they are emphasized in the angular profiles because attention is focused on individual points on the dispersion curve.

### C. Inelastic Angular Profiles

Inelastic angular profiles have been measured for  $0^\circ \leq \theta_s \leq 30^\circ$  with  $2^\circ$  between data points. The primary energy changes by 5 eV between profiles and covers the range  $40 \leq E_p \leq 80$  eV. Such profile sequences have been obtained at 2 eV intervals in energy loss, ranging from 8.4 to 18.4 eV loss. Three of the sequences are presented here in Figs. 9-11. Positions of observed ILEED maxima

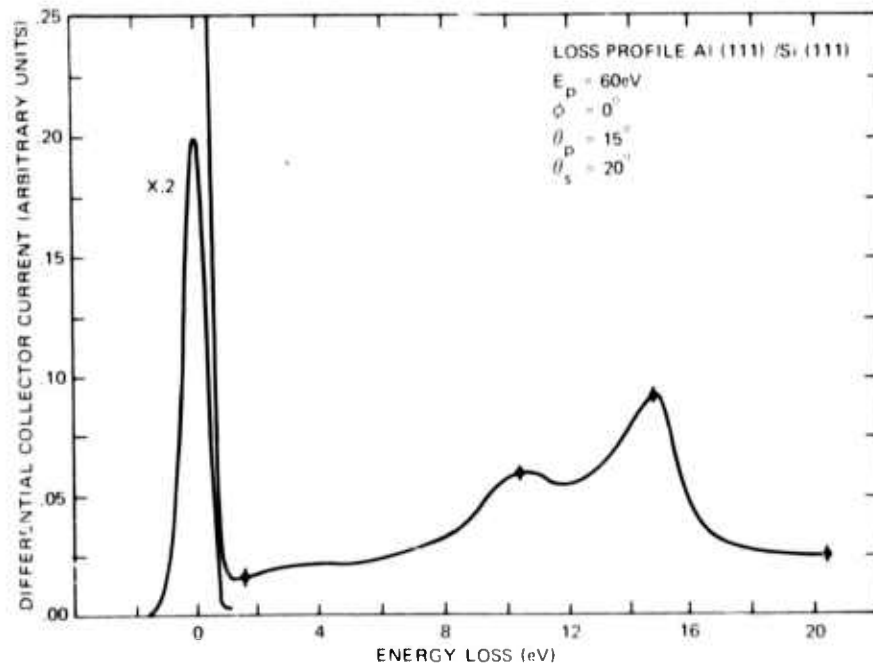


FIGURE 8. Loss profile with collector set  $5^\circ$  from the 00 beam in the direction opposite the normal. The primary energy is the same as in Fig. 7.

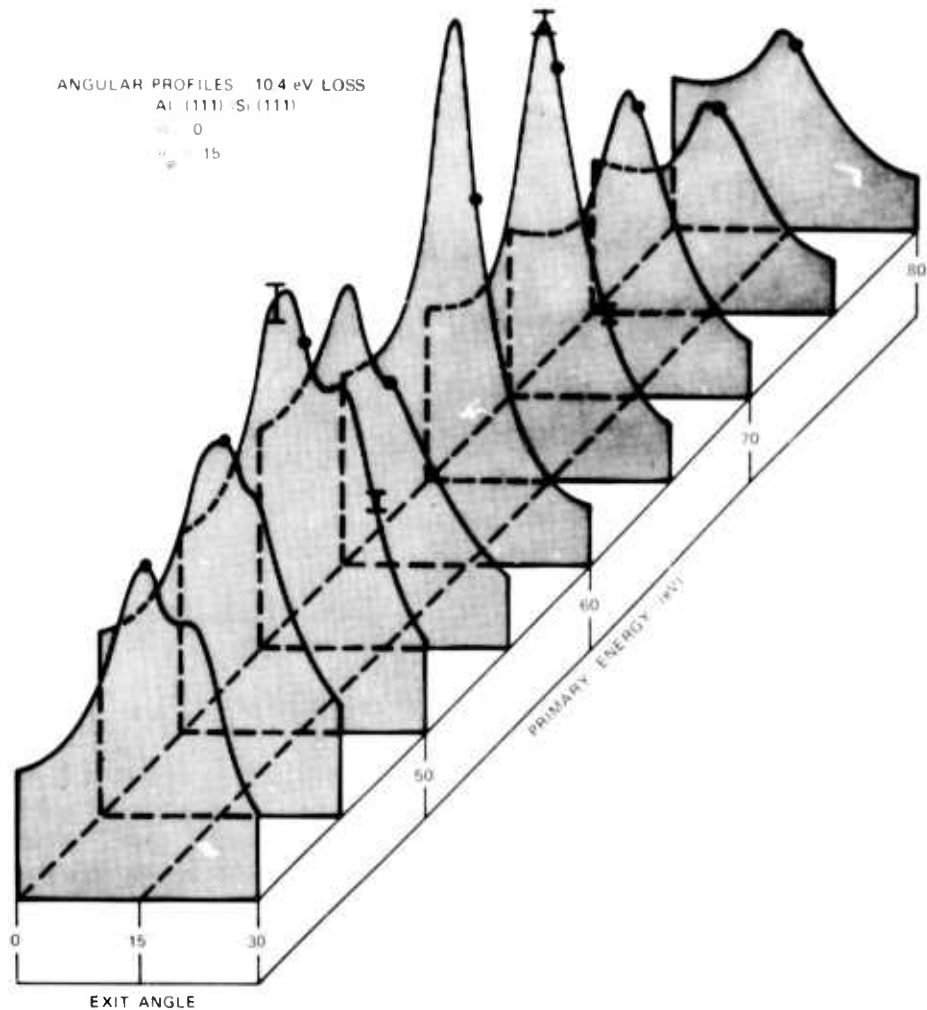


FIGURE 9. Angular profiles at 10.4-eV loss [Al(111)/Si(111)] showing structure arising from the surface plasmon. The exit angle  $\theta_e$  is measured from the normal. Solid dots indicate the position of the LEED beam. Error bars represent rms deviation.  $\phi = 0^\circ$ ,  $\theta_p = 15^\circ$ .

which appear in this data are given in Tables I and II according to their identification in terms of the model. Observed  $E_p$  values are quoted to the nearest multiple of 5 eV. Values enclosed in parentheses represent a shoulder with respect to the pertinent variable rather than a true maximum at that position.

Structure is quite evident in the angular profiles at 8.4-eV loss, which is well below the minimum surface plasmon energy permitted by Eq. (9). Examination of the loss profiles suggests that this structure arises purely from broadening. Increasing the loss to 10.4 eV, which is above the surface plasmon peak in the loss profile of Fig. 6, produces the structure seen in Fig. 9. Here the DL doublet is quite apparent in the 50-eV profile while the LD peak at 60 eV is very prominent. Applying Eq. (10) and the model to the latter, as described above, yields a satisfactory prediction of the observed doublet if some allowance is made for overlap of the two components. However, the high-angle LD maximum predicted for the 65-eV profile is not observed. Predictions obtained from the model based on Eq. (9) are less satisfactory at 10.4-eV loss, but are in substantial agreement with predictions based on Eq. (10) at 12.4- and 14.4-eV losses. For energy losses above 10.4 eV the position of the high-angle DL maxima is not predicted adequately by either method. For the high-angle DL

and LD components the nonconservation of momentum normal to the surface is more pronounced, especially at higher energy losses, as can be seen in Fig. 1(a) and 1(b), respectively. The observed weakness of the corresponding 1LEED maxima suggests that the role of normal momentum conservation is not entirely negligible in surface plasmon excitation, as assumed in the model.

At 12.4-eV loss a hint of the bulk plasmon structure appears, and at 14.4-eV loss this dominates the angular profiles, as seen in Fig. 10. The surface plasmon structure here has moved well away from the LEED beam as a result of the increased surface plasmon momentum, and is visible as a relatively small maximum on the low-angle side of the bulk plasmon structure. The latter structure, on the other hand, lies near the LEED beam as a result of the small bulk plasmon momentum. According to the model, using Eqs. (14) and (15) to evaluate  $K$ , vestigial normal momentum conservation for the bulk plasmon DL process occurs only in our profiles at 18.4-eV loss, which agrees with the lack of corresponding distinct maxima at 50-eV primary energy. At 16.4-eV loss (Fig. 11) the surface plasmon structure at low angles persists,<sup>15</sup> whereas the bulk plasmon structure is substantially diminished. The latter is seen in the LD maximum at 65-eV primary energy, which appears

at a lower angle than in Fig. 10, as a result of the increased plasmon momentum. The high-angle LD maximum is again not observed. Except for a faint bulk plasmon LD maximum the profiles at 18.4-eV loss are essentially featureless. This indicates that the bulk, in contrast to the surface plasmon ILEED intensity, diminishes rapidly with increased energy loss, a result which is also apparent from the loss profiles.

#### D. Plasmon Dispersion

Also included in Tables I and II are the  $K$  values which result from applying Eq. (10) or Eqs. (14) and (15), respectively, to the angular profile data. In Fig. 12 the energy loss  $E$  is plotted against these  $K$  values to illustrate experimentally determined points in the respective dispersion relationships. Equations (9) and (13) are represented here by the dashed curves for comparison.

A least squares quadratic fit to the surface plasmon point (circles), excluding the point at 8.4 eV, yields the solid curve, which represents

$$E(K) = 9.5 + 1.8K + 7.8K^2. \quad (16)$$

The failure of the 8.4-eV point to fall near the curve supports the contention that the structure in the 8.4-eV angular profiles results from broadening. Unfortunately, broadening and the lower limit on  $K$  imposed by energy-

momentum considerations<sup>2</sup> precludes an accurate determination of  $E(K)$  near  $K=0$  based on the angular profiles alone. A more sophisticated analysis, which includes the loss profiles, leads to the expression<sup>7,8</sup>

$$E(K) = 10.1 - 0.7K + 10K^2. \quad (17)$$

Comparing Eqs. (16) and (17) with Eq. (9) shows that the linear coefficient of  $K$  is considerably lower, and the quadratic coefficient considerably higher than anticipated from theory.<sup>10</sup> It should be emphasized that these results apply to a surface plasmon which penetrates only a few lattice constants into the (111) surface. Departure from Eq. (9), which is based on average bulk properties, including electron density, is therefore not surprising.

It is more difficult to infer an accurate dispersion relationship for the bulk plasmon from present measurements. In the first place, as is clear from a comparison of the surface vs bulk plasmon structure in the angular profiles, the bulk plasmon loss maxima are less sharply defined. The lack of DL maxima and the persistence of the surface plasmon structure introduce additional uncertainties. The latter, in particular, makes it difficult to determine from the loss profiles whether the 14.4-eV point is seriously displaced by broadening, similar to the point at 8.4 eV discussed above. The inner potential, which was neglected in the present develop-

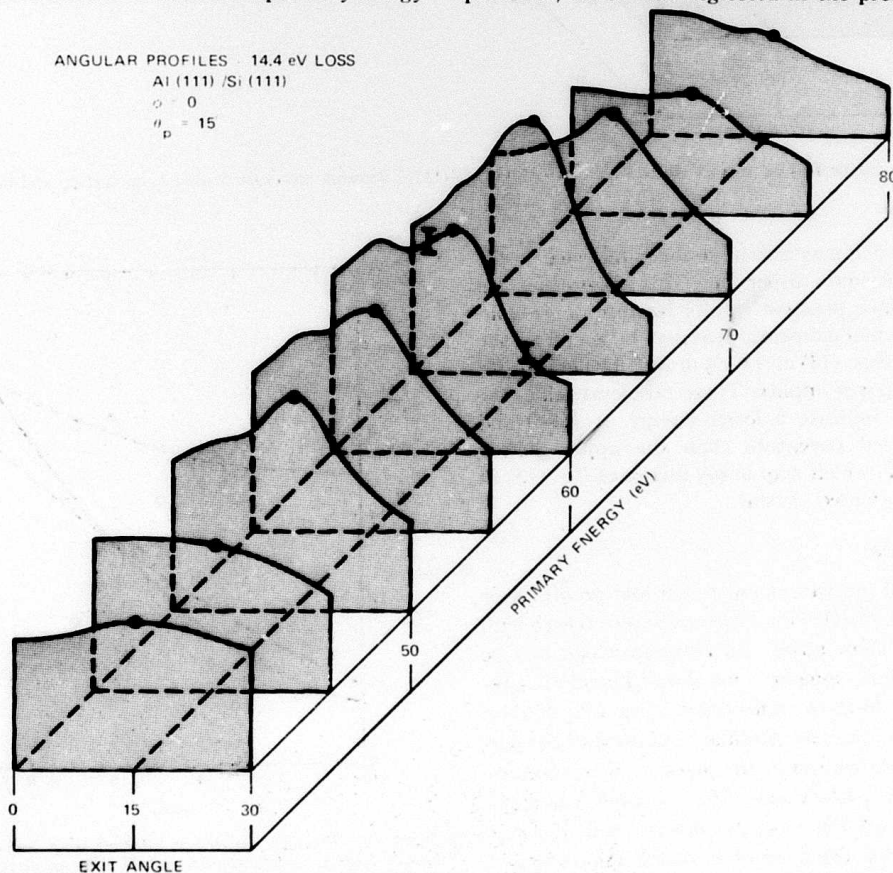


FIGURE 10. Angular profiles at 14.4-eV loss [Al(111)/Si(111)] showing structure arising from surface and bulk plasmons.  $\phi = 0^\circ$ ,  $\theta_p = 15^\circ$ .

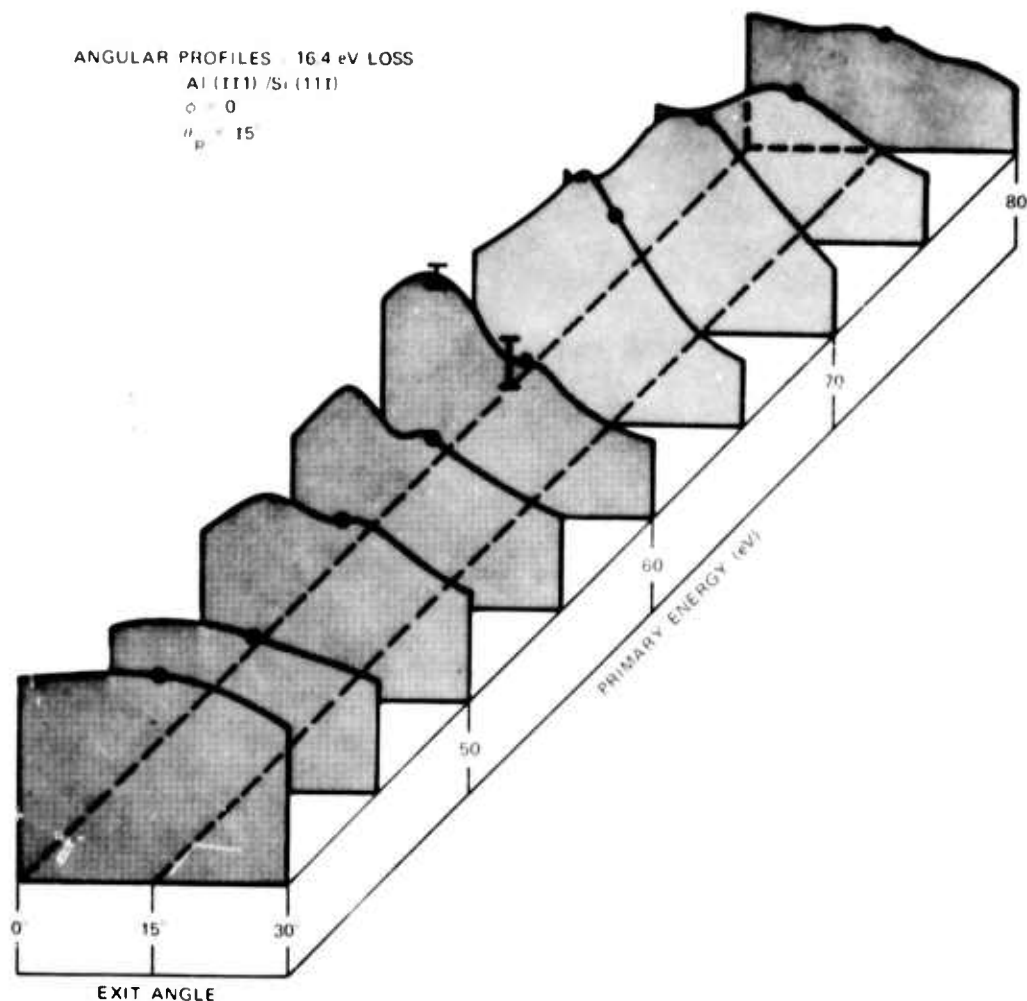


FIGURE 11. Angular profiles at 16.4-eV at 16.4-eV loss [Al(111)/Si(111)] showing structure arising from surface and bulk plasmons.  $\phi = 0^\circ$ ,  $\theta_p = 15^\circ$ .

ment of the model, may also have some influence on the inferred bulk plasmon dispersion.<sup>2</sup> This has no effect on the above surface plasmon results because of nonconservation of normal momentum, as may be seen from the equivalence of Eqs. (13) and (A9) of Ref. 2 when Eq. (8) of the present paper applies. These problems aside, the data generally indicate a lower energy at  $K=0$  and more pronounced curvature than the upper dashed curve in Fig. 12, which may imply failure of Eq. (13) at large  $K$  in an oriented crystal.

#### IV. Conclusions

Experimental inelastic angular and loss profiles near the 00 beam from Al(111) have been measured with high resolution and show structural features which can be related to plasmon momenta by a simple kinematic two-step model of inelastic diffraction. The DL doublet corresponding to the two possible directions of the surface plasmon momentum in the plane of diffraction are clearly visible at 10.4-eV loss. The low-angle LD maximum is in general the most prominent peak and supports the authors' previous observation that, from an experimental standpoint, it provides a new source of

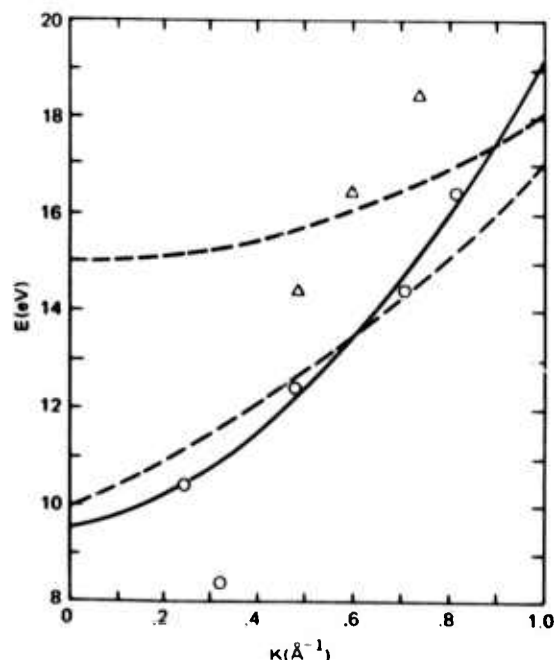


FIGURE 12. Plasmon dispersion inferred from inelastic angular profiles. Circular and triangular points correspond to the surface and bulk plasmon, respectively. Significance of the curves is explained in the text.

precise information on excitation dispersion at large  $K$  values. The two-step model, in its present form, often improperly predicts the high-angle ILEED maxima; a theory which properly represents this aspect of the data has not yet been reported.

The surface plasmon dispersion characteristics inferred from the present data represent the only ones yet available from experiment at large  $K$  value. Significant departure from a theoretical dispersion based on average bulk properties suggests that this surface plasmon characterizes a shallow selvedge peculiar to the clean Al(111) surface. An extension of measurements to other angles, other beams, and other crystal faces would be useful to verify this result, and to eliminate possible sources of systematic error. Of particular concern are instrumental resolution and artifacts of sample preparation. The substrate aging effect observed here gives ample evidence of the latter, and also suggests that a significant increase in sensitivity may be possible with improved sample preparation techniques.

#### Acknowledgments

The authors are grateful to Professor C. B. Duke for preprints and communication of preliminary theoretical

results; to Professor E. Bauer for helpful discussions, and for reviewing the manuscript; and to Maxine J. Booty for an outstanding job of computer programming. Work was supported by Navy Independent Research funding.

#### References

- <sup>1</sup> J. O. Porteus, in *The Structure and Chemistry of Solid Surfaces*, edited by G. Somorjai (Wiley, New York, 1970), p. 12.
- <sup>2</sup> J. O. Porteus and W. N. Faith, *Phys. Rev. B* **2**, 1532 (1970).
- <sup>3</sup> M. P. Seah, *Surface Sci.* **24**, 357 (1971).
- <sup>4</sup> C. B. Duke, A. J. Howsman, and G. E. Laramore, *J. Vac. Sci. Technol.* **8**, 10 (1971).
- <sup>5</sup> C. B. Duke and G. E. Laramore, *Phys. Rev. B* **3**, 3183 (1971); G. E. Laramore and C. B. Duke, *ibid.* **3**, 3198 (1971).
- <sup>6</sup> J. O. Porteus and W. N. Faith, *Proceedings of the Fifth Low-Energy-Electron Diffraction Seminar* (NBS Lecture Notes, Washington, 1971), pp. 81-85.
- <sup>7</sup> C. B. Duke and A. Bagchi, *J. Vac. Sci. Technol.* **9**, 738 (1972).
- <sup>8</sup> A. Bagchi, C. B. Duke, P. J. Feibelman, and J. O. Porteus, *Phys. Rev. Lett.* **27**, 998 (1971).
- <sup>9</sup> H. Raether, *Ergeb. Exakt. Naturwiss.* **38**, 84 (1965).
- <sup>10</sup> D. E. Beck, *Phys. Rev. B* **4**, 1555 (1971).
- <sup>11</sup> E. Bauer, Annual Report for Period 1 February 1968-31 January 1969, NASA Contract No. R-05-030-001, April 1969; E. Bauer, *Z. Physik* **224**, 19 (1969).
- <sup>12</sup> E. Bauer (private communication).
- <sup>13</sup> F. Jona, *IBM J. Res. Develop.* **14**, 444 (1970).
- <sup>14</sup> H. Ehrenreich, H. R. Philipp, and B. Segall, *Phys. Rev.* **132**, 1918 (1963).
- <sup>15</sup> C. B. Duke (private communication).

UNCLASSIFIED

Security Classification

DOCUMENT CONTROL DATA - R & D

(Security classification of title, body of abstract and indexing annotation must be entered when the overall report is classified)

1. ORIGINATING ACTIVITY (Corporate author) <b>Naval Weapons Center China Lake, CA 93555</b>		2a. REPORT SECURITY CLASSIFICATION <b>UNCLASSIFIED</b>	
		2b. GROUP	
3. REPORT TITLE <b>INELASTIC LOW-ENERGY ELECTRON DIFFRACTION MEASUREMENTS ON Al(111)</b>			
4. DESCRIPTIVE NOTES (Type of report and inclusive dates)			
5. AUTHOR(S) (First name, middle initial, last name) <b>J. O. Porteus and W. N. Faith</b>			
6. REPORT DATE <b>March 1973</b>		7a. TOTAL NO. OF PAGES <b>11</b>	7b. NO. OF REFS <b>15</b>
8a. CONTRACT OR GRANT NO. <b>ARPA Order No. 2175</b>		9a. ORIGINATOR'S REPORT NUMBER(S) <b>NWC TP 5493</b>	
b. PROJECT NO. <b>ZR 00001, Task Area ZR 01102</b>			
c.		9b. OTHER REPORT NO(S) (Any other numbers that may be assigned this report)	
d.			
10. DISTRIBUTION STATEMENT <b>DISTRIBUTION LIMITED TO U.S. GOVERNMENT AGENCIES ONLY; TEST AND EVALUATION; 23 FEBRUARY 1973. OTHER REQUESTS FOR THIS DOCUMENT MUST BE REFERRED TO THE NAVAL WEAPONS CENTER</b>			
11. SUPPLEMENTARY NOTES		12. SPONSORING MILITARY ACTIVITY <b>Naval Material Command Director of Laboratory Programs Washington, D. C. 20360</b>	
13. ABSTRACT <p>An experimental study has been made of electrons in the energy range 40-80 eV; inelastically scattered and diffracted from a clean Al(111) surface. The surface is prepared by epitaxial vapor deposition on a Si(111) single-crystal surface in ultrahigh vacuum immediately preceding the measurements. The inelastic electron intensity at a given energy loss and angle is obtained as the energy derivative of the amplified electron current from a Faraday collector having a retarding field analyzer and limited angular acceptance. The energy derivative comes from the digitally computed average of a repeatedly measured difference in dc signal accompanying a fixed increment in retarding field. Using this method inelastic angular and loss profiles at 15° incidence have been obtained in the vicinity of a Bragg maximum of the 00 elastic beam. The profiles show structure related to the surface and volume plasmon momenta by a two-step model of inelastic diffraction. Dispersion data inferred by applying this model to the "loss-before-diffraction" structure are compared with results from other sources. The surface plasmon dispersion obtained from inelastic low energy electron diffraction measurements shows promise as a new means of characterizing solid crystalline surfaces.</p>			

DD FORM 1473

1 NOV 65

(PAGE 1)

S/N 0101-807-6801

UNCLASSIFIED

Security Classification

14

KEY WORDS

LINK A

LINK B

LINK C

ROLE

WT

ROLE

WT

ROLE

WT

Inelastic Diffraction  
Crystal Surfaces  
Aluminum  
Surface Plasmons

ABSTRACT CARD

Naval Weapons Center

Inelastic Low-Energy Electron Diffraction Measurements on Al(111), by J. O. Porteus and W. N. Faith, China Lake, Calif., NWC, March 1973. 11 pp. (NWC TP 5493 (a reprint from J VAC SCI TECHNOL, Vol. 9, No. 3, May-June 1972), publication UNCLASSIFIED.)

An experimental study has been made of electrons in the energy range 40-80 eV, inelastically scattered and diffracted from a clean Al(111) surface. The surface is prepared by epitaxial vapor deposition

○ 2 cards, 8 copies (Over)

Naval Weapons Center

Inelastic Low-Energy Electron Diffraction Measurements on Al(111), by J. O. Porteus and W. N. Faith, China Lake, Calif., NWC, March 1973. 11 pp. (NWC TP 5493 (a reprint from J VAC SCI TECHNOL, Vol. 9, No. 3, May-June 1972), publication UNCLASSIFIED.)

An experimental study has been made of electrons in the energy range 40-80 eV, inelastically scattered and diffracted from a clean Al(111) surface. The surface is prepared by epitaxial vapor deposition

○ 2 cards, 8 copies (Over)

Naval Weapons Center

Inelastic Low-Energy Electron Diffraction Measurements on Al(111), by J. O. Porteus and W. N. Faith, China Lake, Calif., NWC, March 1973. 11 pp. (NWC TP 5493 (a reprint from J VAC SCI TECHNOL, Vol. 9, No. 3, May-June 1972), publication UNCLASSIFIED.)

An experimental study has been made of electrons in the energy range 40-80 eV, inelastically scattered and diffracted from a clean Al(111) surface. The surface is prepared by epitaxial vapor deposition

○ 2 cards, 8 copies (Over)

Naval Weapons Center

Inelastic Low-Energy Electron Diffraction Measurements on Al(111), by J. O. Porteus and W. N. Faith, China Lake, Calif., NWC, March 1973. 11 pp. (NWC TP 5493 (a reprint from J VAC SCI TECHNOL, Vol. 9, No. 3, May-June 1972), publication UNCLASSIFIED.)

An experimental study has been made of electrons in the energy range 40-80 eV, inelastically scattered and diffracted from a clean Al(111) surface. The surface is prepared by epitaxial vapor deposition

○ 2 cards, 8 copies (Over)

NWC TP 5493

on a Si(111) single-crystal surface in ultrahigh vacuum immediately preceding the measurements. The inelastic electron intensity at a given energy loss and angle is obtained as the energy derivative of the amplified electron current from a Faraday collector having a retarding field analyzer and limited angular acceptance. The energy derivative comes from the digitally computed average of a repeatedly measured difference in dc signal accompanying a fixed increment in retarding field. Using this method inelastic angular and loss profiles at 15° incidence have been obtained in the vicinity of a Bragg maximum

(Contd. on Card 2)

NWC TP 5493

on a Si(111) single-crystal surface in ultrahigh vacuum immediately preceding the measurements. The inelastic electron intensity at a given energy loss and angle is obtained as the energy derivative of the amplified electron current from a Faraday collector having a retarding field analyzer and limited angular acceptance. The energy derivative comes from the digitally computed average of a repeatedly measured difference in dc signal accompanying a fixed increment in retarding field. Using this method inelastic angular and loss profiles at 15° incidence have been obtained in the vicinity of a Bragg maximum

(Contd. on Card 2)

NWC TP 5493

on a Si(111) single-crystal surface in ultrahigh vacuum immediately preceding the measurements. The inelastic electron intensity at a given energy loss and angle is obtained as the energy derivative of the amplified electron current from a Faraday collector having a retarding field analyzer and limited angular acceptance. The energy derivative comes from the digitally computed average of a repeatedly measured difference in dc signal accompanying a fixed increment in retarding field. Using this method inelastic angular and loss profiles at 15° incidence have been obtained in the vicinity of a Bragg maximum

(Contd. on Card 2)

NWC TP 5493

on a Si(111) single-crystal surface in ultrahigh vacuum immediately preceding the measurements. The inelastic electron intensity at a given energy loss and angle is obtained as the energy derivative of the amplified electron current from a Faraday collector having a retarding field analyzer and limited angular acceptance. The energy derivative comes from the digitally computed average of a repeatedly measured difference in dc signal accompanying a fixed increment in retarding field. Using this method inelastic angular and loss profiles at 15° incidence have been obtained in the vicinity of a Bragg maximum

(Contd. on Card 2)

ABSTRACT CARD

Naval Weapons Center

Inelastic Low-Energy . . . (Card 2)  
of the 00 elastic beam. The profiles show structure related to the surface and volume plasmon momenta by a two-step model of inelastic diffraction. Dispersion data inferred by applying this model to the "loss-before-diffraction" structure are compared with results from other sources. The surface plasmon dispersion obtained from inelastic low energy electron diffraction measurements shows promise as a new means of characterizing solid crystalline surfaces.

NWC TP 5493

Naval Weapons Center

Inelastic Low-Energy . . . (Card 2)  
of the 00 elastic beam. The profiles show structure related to the surface and volume plasmon momenta by a two-step model of inelastic diffraction. Dispersion data inferred by applying this model to the "loss-before-diffraction" structure are compared with results from other sources. The surface plasmon dispersion obtained from inelastic low energy electron diffraction measurements shows promise as a new means of characterizing solid crystalline surfaces.

NWC TP 5493

Naval Weapons Center

Inelastic Low-Energy . . . (Card 2)  
of the 00 elastic beam. The profiles show structure related to the surface and volume plasmon momenta by a two-step model of inelastic diffraction. Dispersion data inferred by applying this model to the "loss-before-diffraction" structure are compared with results from other sources. The surface plasmon dispersion obtained from inelastic low energy electron diffraction measurements shows promise as a new means of characterizing solid crystalline surfaces.

NWC TP 5493

Naval Weapons Center

Inelastic Low-Energy . . . (Card 2)  
of the 00 elastic beam. The profiles show structure related to the surface and volume plasmon momenta by a two-step model of inelastic diffraction. Dispersion data inferred by applying this model to the "loss-before-diffraction" structure are compared with results from other sources. The surface plasmon dispersion obtained from inelastic low energy electron diffraction measurements shows promise as a new means of characterizing solid crystalline surfaces.

NWC TP 5493